photochem

MDPI

Article

Electrospun Carbon Nanofibers Decorated with Ag_3PO_4 Nanoparticles: Visible-Light-Driven Photocatalyst for the Photodegradation of Methylene Blue

Gopal Panthi [1] and Mira Park [1,2,*]

[1] Carbon Composite Energy Nanomaterials Research Center, Woosuk University, Wanju, Chonbuk 55338, Korea; gopalpanthi2003@gmail.com
[2] Woosuk Institute of Smart Convergence Life Care (WSCLC), Woosuk University, Wanju, Chonbuk 55338, Korea
* Correspondence: wonderfulmira@woosuk.ac.kr; Tel.: +82-63-290-1536

Abstract: For the first time, heterostructures of electrospun carbon nanofibers decorated with Ag_3PO_4 nanoparticles (Ag_3PO_4/CNFs) were successfully fabricated by the combination of simple and versatile electrospinning technique followed by carbonization and incorporation of Ag_3PO_4 nanoparticles via colloidal and precipitation synthesis approaches. The as-fabricated heterostructures were characterized by FESEM with EDS, XRD, TEM with HRTEM, FTIR and UV-vis diffuse reflectance spectroscopy. Experimental results revealed that the heterostructure obtained by colloidal synthesis approach (Ag_3PO_4/CNFs-1) was decorated with small-sized (~20 nm) and uniformly distributed Ag_3PO_4 nanoparticles on the surface of CNFs without any evident agglomeration, while in the heterostructure obtained by the precipitation synthesis approach (Ag_3PO_4/CNFs-2), CNFs were decorated with agglomerated and bigger-sized Ag_3PO_4 nanoparticles. The visible-light-driven photocatalytic investigation signified that the Ag_3PO_4/CNFs-1 heterostructure can exhibit higher performance towards the photodegradation of MB dye solution compared to the Ag_3PO_4/CNFs-2 heterostructure, which could be attributed to the synergistic effect between the uniformity and small size of Ag_3PO_4 nanoparticles and CNFs that can serve as a conductivity network to prevent the recombination of charge carriers. Moreover, the mechanism of the photocatalytic activity as-prepared heterostructure is proposed.

Keywords: electrospinning; carbon composite nanofibers; water pollution; Ag_3PO_4; photocatalyst; visible light

check for updates

Citation: Panthi, G.; Park, M. Electrospun Carbon Nanofibers Decorated with Ag_3PO_4 Nanoparticles: Visible-Light-Driven Photocatalyst for the Photodegradation of Methylene Blue. *Photochem* **2021**, *1*, 345–357. https://doi.org/10.3390/photochem1030022

Academic Editor: Vincenzo Vaiano

Received: 1 September 2021
Accepted: 8 October 2021
Published: 10 October 2021

1. Introduction

Photocatalysis, a "green technique", has been accepted as a potential remedy for the removal of organic pollutants from wastewater [1]. The discovery of the electrochemical photocatalysis of water at TiO_2 electrode by Honda and Fujishima [2] has inspired researchers working in the field of photocatalysis to design and synthesize semiconductor-based photocatalysts. Hence, a number of semiconductor-based photocatalysts such as metal oxides, sulfides and composites have been studied so far [3–6]. In particular, intense research works are focused on the fabrication of visible-light-driven photocatalysts to avoid the cost of UV light and create a comfortable environment for all living beings [7–10]. On that note, Ye and coworkers [11] carried out a breakthrough work to study the photocatalytic activity of silver orthophosphate (Ag_3PO_4) towards water splitting and decomposition of organic contaminants in aqueous solution under visible light irradiation. Afterwards, Ag_3PO_4 as a photocatalyst has attracted much more attention for the removal of various types of organic contaminants from wastewater [12–14]. Ag_3PO_4 is a promising semiconductor material being used as an efficient photocatalyst to achieve significantly higher photocatalytic activity utilizing visible light, but its application is limited due to photocorrosion under repetitive use when used without sacrificial reagent [11].

Indeed, the process of photocorrosion is the insurmountable problem that mostly occurs in silver-based catalysts [15,16]. In this connection, various attempts have been made for designing and developing a Ag_3PO_4-based photocatalyst with a sufficient charge separation ability and high photocatalytic stability in the visible light region either by doping SO_4^- ions [17] and coupling with other semiconductor/s [18–20] or by fabricating composites with graphene [21–23], carbon nanotubes [24,25], and non-metallic adsorbent [26]. However, the effect of the incorporation of Ag_3PO_4 nanoparticles on the surface of carbon nanofibers (CNFs) to enhance its photocatalytic performance has been rarely reported [27]. Due to its one-dimensional structure, high specific surface area, good electrical conductivity and high chemical stability, the use of CNFs in the form of scaffold/supporters as well as ideal electron pathways has attracted great interest in recent years [28,29]. Additionally, some reports have demonstrated that CNFs are capable of capturing electrons and serve as the conductivity network by transforming photogenerated electrons along their longitude conductive length [30,31]. Based on these unique properties of CNFs, fabrication of Ag_3PO_4/CNFs heterostructures could be an ideal strategy for hindering the recombination of photogenerated electrons and holes thereby improving the photocatalytic performance of Ag_3PO_4. The introduction of surface functional groups on CNFs that can act as anchoring sites for nanoparticles to obtain uniform dispersion is another important task. Therefore, various approaches have been proposed to introduce surface functional groups on CNFs, such as chemical oxidation [32], air oxidation [33], plasma treatment [34], and electrochemical oxidation [35]. Among these, the chemical oxidation of CNFs by acid treatment is being used widely to introduce oxygen containing functional groups under different conditions [36].

Herein, we report a facile approach to fabricate novel organic–inorganic heterostructures composed of functionalized CNFs and Ag_3PO_4 nanoparticles by the combination of carbonization of electrospun precursor PAN nanofibers and decoration of Ag_3PO_4 nanoparticles on the surface of functionalized CNFs following colloidal and precipitation synthesis approaches. To the best of our knowledge, there has been no report on the fabrication and visible light photocatalytic properties of Ag_3PO_4/CNFs heterostructures with sufficient electron–hole separation ability. The experimental results showed that the Ag_3PO_4/CNFs heterostructure obtained by the colloidal synthesis approach exhibited higher photocatalytic activity in the visible light region compared to the heterostructure obtained by the precipitation synthesis approach. Additionally, due to the high length-to-diameter ratio of CNFs, the as-fabricated Ag_3PO_4/CNFs heterostructures could be separated by the sedimentation process. Furthermore, we present a study on the effect of solution concentrations on the morphology of nanostructures (nanoagglomerates or nanoparticles) as well as their size.

2. Materials and Methods

2.1. Materials

Polyacrylonitrile (PAN, MW-150000), silver nitrate ($AgNO_3$), sodium phosphate dibasic dihydrate ($Na_2HPO_4.2H_2O$), and methylene blue (MB) were purchased from Sigma-Aldrich, St. Louis, MO, USA. *N*,*N*-dimethylformamide (DMF) and nitric acid (HNO_3, 65%) were purchased from Daejung Chemicals, Seoul, Korea. All the chemicals were used as received.

2.2. Fabrication of Carbon Nanofibers

A 10 wt% of PAN solution was prepared by dissolving required amount of PAN powder in DMF at room temperature under constant magnetic stirring for 12 h. The precursor solution was then loaded into a plastic syringe equipped with metallic needle connected to a high-voltage power supply (high voltage power supply, HV 30/ESN-HV30N, Nano NC, Seoul, Korea) capable of producing DC voltages from 0 to 30 kV and electrospun at 18 kV with a constant flow rate of 1 mL/h through a syringe pump. The nanofibers were collected on aluminum foil wrapped over a rotating drum collector at

15 cm apart from the needle tip. All experiments were conducted at room temperature and atmosphere pressure. The as-fabricated precursor PAN-nanofibers were vacuum dried at 70 °C for 12 h in order to remove the residual solvent. For carbonization, the vacuum-dried PAN-nanofibers were placed in a tube furnace and stabilized in air at 250 °C for 1 h with a heating rate of 1 °C/min, then carbonized in nitrogen up to 800 °C at a rate of 5 °C/min, and finally cooled to room temperature to the obtained electrospun carbon nanofibers (CNFs).

2.3. Fabrication of Ag_3PO_4/CNFs Heterostructures

At first, the oxidation of CNFs was carried out by treating with HNO_3 (65%) at 45 °C for 12 h followed by washing with distilled water until the pH became 7 then dried at 80 °C for 9 h. Afterwards, Ag_3PO_4/CNFs heterostructures were fabricated following two synthetic approaches, i.e., colloidal and precipitation synthesis approach simply by adjusting the concentrations of reactants ($Na_2HPO_4.2H_2O$ and $AgNO_3$) as described by Khan et al. [37]. In the colloidal synthesis approach, 0.1 g of acid-treated CNFs were added to 100 mL of (0.02 M) $AgNO_3$ solution and stirred for 30 min. Then, 100 mL of (0.02 M) Na_2HPO_4 solution was added to the CNFs/$AgNO_3$ mixture solution in a dropwise manner under constant stirring. The product was collected and washed with distilled water and ethanol followed by vacuum drying at 70 °C for 12 h. Likewise, in the precipitation synthetic approach, the concentration of reactants was adjusted to 0.1 M, while the post-treatment process of the mixture was the same as that of the colloidal synthesis approach. The schematic illustration for the fabrication of Ag_3PO_4/CNFs heterostructures is given in Figure 1. For the convenience of description, the Ag_3PO_4/CNFs heterostructures were herein called Ag_3PO_4/CNFs-1 and Ag_3PO_4/CNFs-2 synthesized from the colloidal synthesis approach and precipitation synthesis approach, respectively.

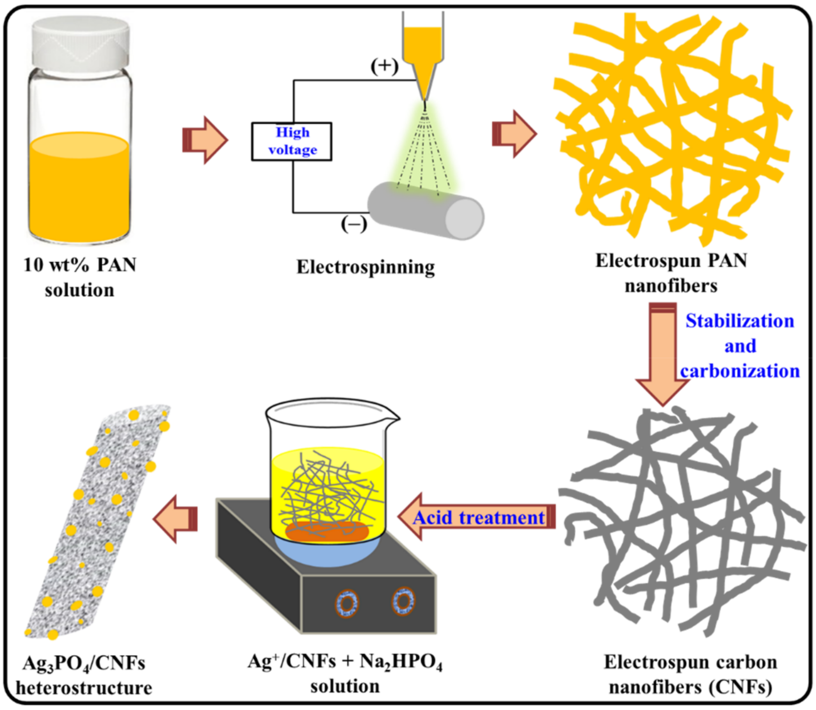

Figure 1. Schematic illustration for the fabrication of Ag_3PO_4/CNFs heterostructures.

2.4. Characterization

A field emission scanning electron microscope (FESEM, GeminiSEM 500, Carl Zeiss Microscopy GmbH, 73,447 Oberkochen, Germany) and transmission electron microscope (TEM/HR-TEM; JEM-2200FS, JEOL Ltd., Akishima, Tokyo, Japan) equipped with energy dispersive X-ray spectroscopy (EDS) were used to characterize the morphology and distribution of nanoparticles on the surface CNFs. EDS being attached to FESEM was used to analyze the composition of samples. X-ray diffraction (XRD) measurement was carried out to characterize the phase and crystallinity of as-prepared samples using an X-ray diffractometer (XRD, Empyrean, PANAlytical, Eindhoven 5651 GH, the Netherlands) with Cu Kα (λ = 1.540 Å) radiation over Bragg angles ranging from 10° to 80°. Fourier transform infrared (FTIR) spectroscopy was performed to characterize the bonding configurations of CNFs with nanoparticles by using Fourier-transform infrared (FT-IR, FT/IR-4200, Jasco, international Co., Ltd., Hachioji, Tokyo, 193-0835, Japan). UV-vis diffuse reflectance spectra (DRS) were measured using a UV-vis spectrophotometer (UV-2600 240 EN, SHIMADZU CORPORATION, Kyoto, Japan).

2.5. Photocatalytic Test

Photocatalytic performances of different photocatalysts were examined by observing the degradation of MB dye solution. For comparison, standard photocatalyst such as Evonic P25 TiO_2 was also employed in this study. All the experiments were performed at room temperature using a solar simulator (DYX300P, DYE TECH Co., Seoul, Korea) equipped with an internal xenon lamp and provided with a UV cut-off filter. Typically, suspension of each photocatalyst was prepared by dispersing 150 mg of photocatalyst in 50 mL of dye solution with initial concentration of 10 ppm and magnetically stirred in the dark for 30 min to attain adsorption/desorption equilibrium between dye and photocatalyst. The suspension was then irradiated with visible light (λ > 420 nm) produced from a 200 W xenon lamp under constant magnetic stirring. Aliquots were taken at 10 min time interval and the concentration of dye solution was measured using a UV-Vis spectrophotometer (HP 8453 UV-Vis spectroscopy system, Hudson, MA, USA).

3. Results and Discussion

The surface morphology of the precursor PAN nanofibers, CNFs and Ag_3PO_4/CNFs heterostructures were observed in FESEM images (Figure 2). As shown in Figure 2a, electrospun precursor PAN nanofibers exhibited uniform and continuous nanofibers with random orientation forming an interwoven 3-D network without the presence of any beads. The average diameter of these precursor nanofibers was found to be 320 nm. However, after carbonization of precursor PAN nanofibers, it could be clearly seen that CNFs still kept their nanofibrous morphology with a relatively smooth surface and random orientation without the presence of any secondary nanostructures. The average diameter of the CNFs was found to have decreased to 240 nm (Figure 2b). This decrease in fiber diameter can be attributed to the shrinkage in volume of PAN nanofibers due to weight loss during carbonization process. This is because during carbonization evaporation of residual solvent, removal of unwanted elements, densification of carbon, and evolution of the various gases such as H_2O, N_2, HCN, etc. from the precursor PAN nanofibers takes place, resulting in a decrease in fiber diameter [38,39].

After fabrication of heterostructures, both the samples remained with nanofibrous morphology. However, the surface of CNFs was no longer smooth due to growth of secondary Ag_3PO_4 nanoparticles (Figure 2c,d). High-magnification FESEM image of Ag_3PO_4/CNFs-1 heterostructure (inset of Figure 2c) depicted the uniform distribution spherical Ag_3PO_4 nanoparticles with an average size of 20 nm grown on the surface of CNFs without any evident aggregation offering a high level of exposure of the nanoparticle surface; however, the nanoparticles are not visible in low-magnification images (Figure 2c). On the other hand, in the Ag_3PO_4/CNFs-2 heterostructure, the Ag_3PO_4 nanoparticles with a bigger size were not evenly distributed across the surface of CNFs and found in agglomerated form, causing lesser exposure of their effective surface (Figure 2d). Figure 2e,f are the EDS spectra of CNFs and Ag_3PO_4/CNFs-1 heterostructure, respectively. It was indicated that C and O elements existed in pure CNFs, while C, O, Ag, and P elements existed in Ag_3PO_4/CNFs-1 heterostructure, confirming the successful fabrication of Ag_3PO_4/CNFs heterostructures.

Figure 3 represents the elemental mapping of the Ag_3PO_4/CNFs-1 heterostructure; as shown in the figure, carbon (Figure 3b) and oxygen (Figure 3e) have high density as they are incorporated in CNFs; however, silver (Figure 3c) and phosphorus (Figure 3d) have relatively low density. Additionally, from the elemental mapping, one can suggest the formation of Ag_3PO_4 nanoparticles on the CNFs surface.

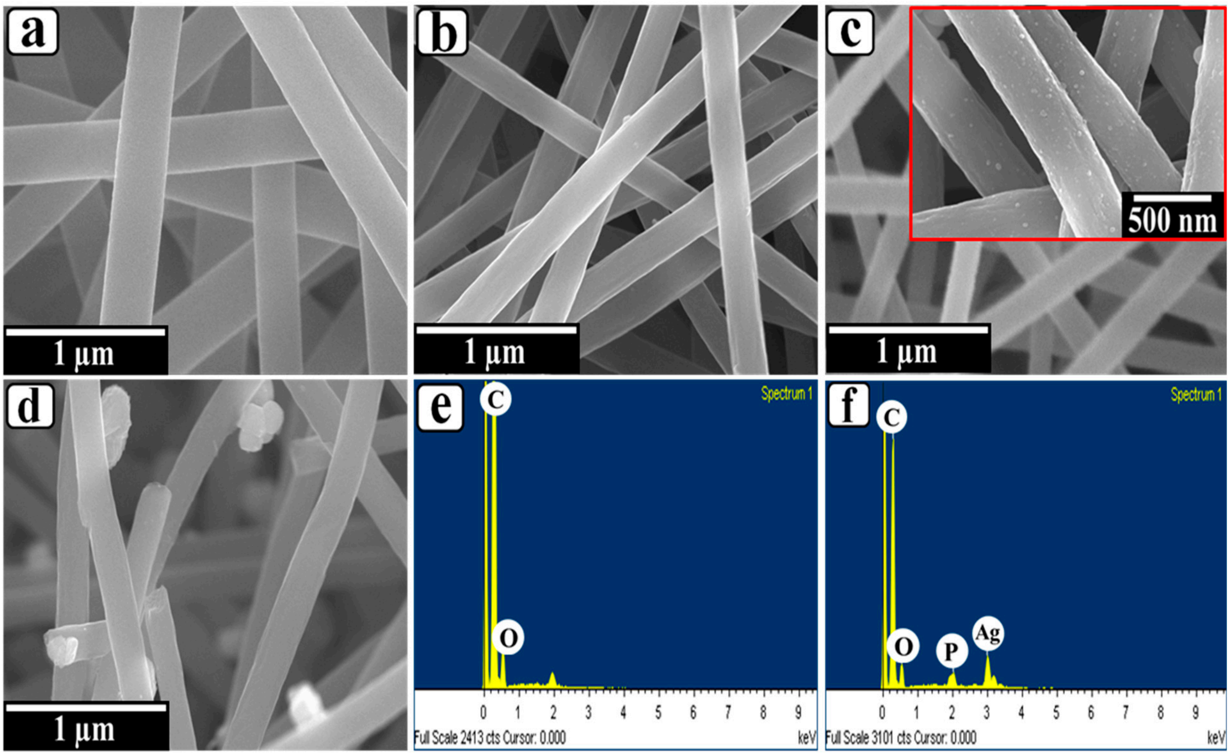

Figure 2. FESEM images; (**a**) precursor PAN nanofibers, (**b**) CNFs, (**c**) Ag_3PO_4/CNFs-1 heterostructure, and (**d**) Ag_3PO_4/CNFs-2 heterostructure. Panel (**e**,**f**) represent FESEM-EDS of CNFs, and Ag_3PO_4/CNFs-1 heterostructure, respectively. Inset; high-magnification FESEM image of Ag_3PO_4/CNFs-1 heterostructure.

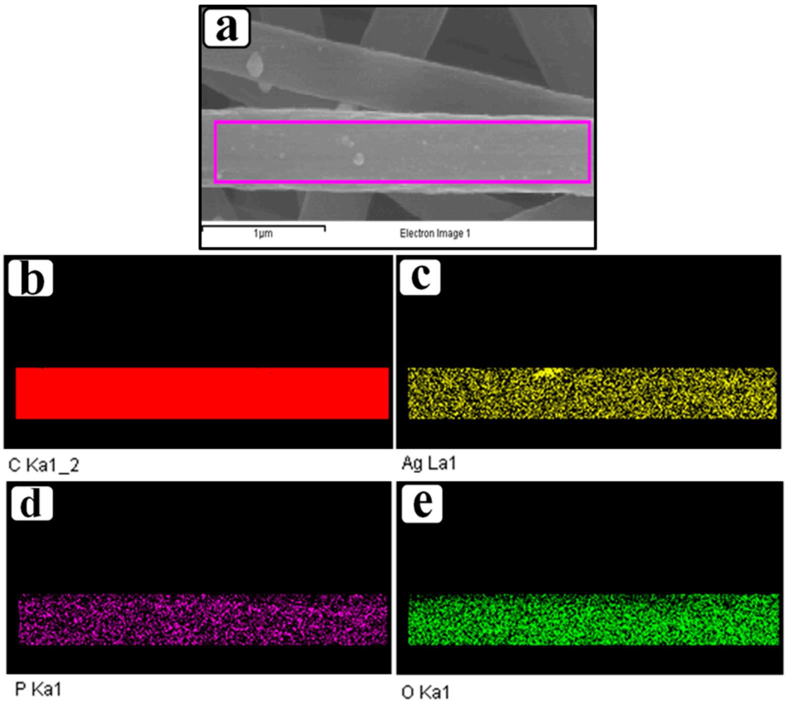

Figure 3. Elemental mapping analysis; (**a**) Ag_3PO_4/CNFs-1 heterostructure, (**b**) carbon, (**c**) silver, (**d**) phosphorus, and (**e**) oxygen elements.

XRD analysis of different samples (Ag_3PO_4 powder, CNFs, Ag_3PO_4/CNFs-1 heterostructure, and Ag_3PO_4/CNFs-2 heterostructure) was carried out to characterize their composition and crystal structure (Figure 4). The broad peak centered at around 25° was attributed to the (002) plane of the carbon structure in the CNFs, Ag_3PO_4/CNFs-2, and Ag_3PO_4/CNFs-2 (Figure 4b–d). Compared to the CNFs, the diffraction peaks at 2θ of 20.879°, 29.700°, 33.300°, 36.581°, 47.799°, 52.682°, 55.019°, 57.280°, 61.658°, and 71.898° in Ag_3PO_4 powder, Ag_3PO_4/CNFs-1, and Ag_3PO_4/CNFs-2 were attributed to the crystal planes of (110), (200), (210), (211), (310), (222), (320), (321), (400), (421) and (332) of Ag_3PO_4 (JCPDS card No: 74-0911), respectively (Figure 4a, c, d) [40]. Furthermore, no peaks for any other impurities were observed. Therefore, these results suggested that both the heterostructures were composed of CNFs and Ag_3PO_4 nanoparticles with high crystallinity and purity, which was also justified by FESEM-EDS.

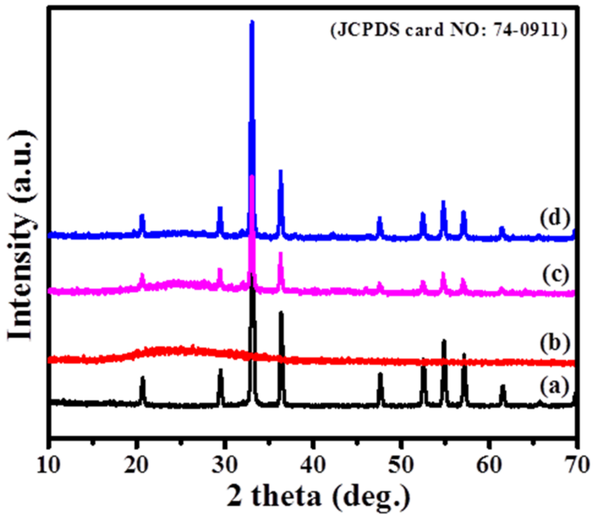

Figure 4. XRD patterns; (**a**) Ag_3PO_4 powder, (**b**) CNFs, (**c**) Ag_3PO_4/CNFs-1 heterostructure, and (**d**) Ag_3PO_4/CNFs-2 heterostructure.

The fiber morphology and degree of dispersion of nanoparticles on the surface of CNFs were observed by HR/TEM analysis (Figure 5). Figure 5a represents a typical TEM image of CNF with nanofibrous morphology possessing a relatively smooth surface as described in FESEM analysis. It is noteworthy that the morphology of CNFs obtained after acid treatment was also consistent and well-retained (inset, Figure 5a). As compared to the CNFs (Figure 5a), the heterostructure (Ag_3PO_4/CNFs-1) exhibited numerous Ag_3PO_4 nanoparticles uniformly distributed and successfully loaded on the surface of CNFs (Figure 5b). The average size of Ag_3PO_4 nanoparticles was found to be 20 nm. More interestingly, the sonication process conducted during the sample preparation for TEM analysis did not cause the Ag_3PO_4 nanoparticles decrease of the CNFs. This indicated that Ag_3PO_4 nanoparticles were successfully grown on the surface of CNFs with strong attachment. Moreover, highly magnified TEM images of the Ag_3PO_4/CNFs-1 heterostructure obtained from the marked area in Figure 5b is shown in Figure 5 c in order to display the attachment of colloidal nanoparticles with the CNFs surface. At the same time, the perfectly crystalline structure of Ag_3PO_4 nanoparticle was observed by HR-TEM image (Figure 5d) recorded from the marked area in Figure 5c. As shown in the figure, the inter planer spacing of 0.299 nm and 0.268 nm corresponding to (200) and (210) crystallographic planes of Ag_3PO_4 nanoparticle were clearly observed revealing its excellent crystallinity. Additionally, the heterojunction displayed that Ag_3PO_4 nanoparticles were attached on the surface of CNF having disordered stacking features indicating its low crystallinity.

In order to analyze the interaction between CNFs and inorganic phase, FTIR analysis was performed; the results are displayed in Figure 6. The IR absorption spectra of Ag_3PO_4 powder (Figure 6a) were compared with that of acid treated CNFs (Figure 6b) and Ag_3PO_4/CNFs-1 heterostructure (Figure 6c). As depicted in the figure, the broad absorption band centered at about 3200 cm^{-1} for Ag_3PO_4 powder or Ag_3PO_4/CNFs heterostructure and a strong absorption band at about 1660 cm^{-1} for Ag_3PO_4 powder were attributed to the stretching vibration of O-H and bending vibration of H-O-H of water molecules, respectively. Furthermore, for Ag_3PO_4 powder, two absorption bands centered at about 1055 cm^{-1} and 1400 cm^{-1} could be assigned to the molecular vibrations of $PO_4{}^{3-}$ [41] and the stretch of the doubly bonded oxygen P=O [42]. For CNFs, a strong broad band was observed at about 3400–3500 cm^{-1}, which might be attributed to the bending vibration of absorbed water molecule and stretching vibration of -OH groups [43]. Similarly, two bands obtained at about 1200 cm^{-1} and 1580 cm^{-1} were due to the C-C stretching vibration [44,45] and carboxylic stretching COO^- vibration [46]. Hence, FTIR analysis clearly showed that the CNFs were -COOH functionalized; however, their peak intensities in the Ag_3PO_4/CNFs heterostructures were found to be decreased after the growth of Ag_3PO_4 nanoparticles on CNFs surface. Additionally, in the heterostructures, the bands corresponding to $PO_4{}^{3-}$ and P=O were observed with a decrease in their peak intensities, suggesting that the carboxylic groups might play a significant role for the nucleation sites during ion exchange reaction.

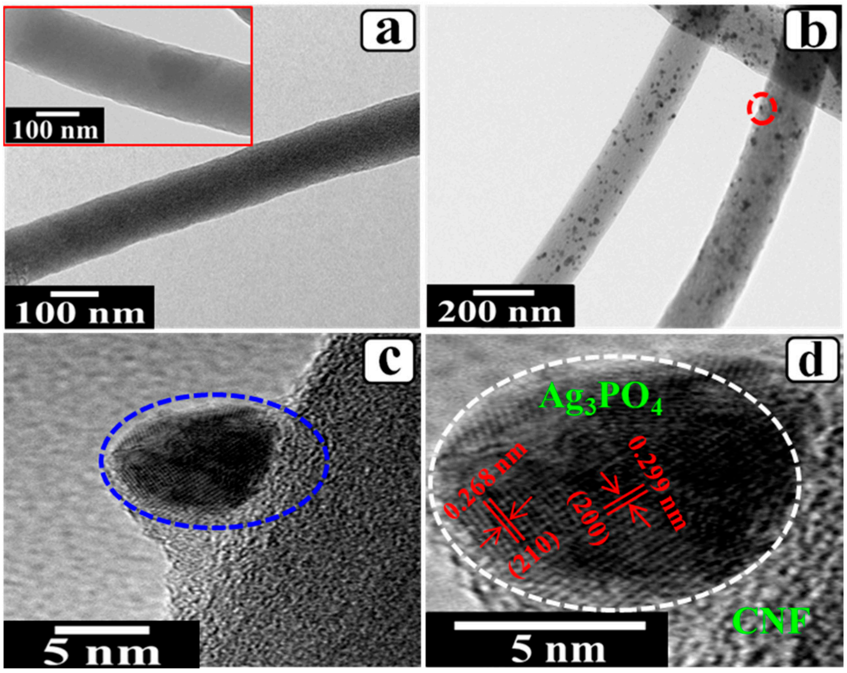

Figure 5. TEM images; (**a**) CNF, (**b**) Ag_3PO_4/CNFs-1heterostructure, (**c**) magnified TEM image of heterojunction region of red circled area for (**b**), and (**d**) HR-TEM image of blue circled area for (**c**). Inset, TEM image of acid-treated CNF.

Since the catalytic performances of any photocatalyst depends on its optical absorption properties, UV-vis diffusive reflectance spectra of Ag_3PO_4 powder and Ag_3PO_4/CNFs heterostructures were analyzed to investigate their optical properties; the results are presented in Figure 7. The pure Ag_3PO_4 powder could absorb light with a wavelength at around 520 nm (Figure 7a) and exhibit strong absorption in the visible range as reported before [47]. In the case of heterostructures, Ag_3PO_4/CNFs-1 (Figure 7b) also exhibited excellent absorption in the visible region with a wavelength at around 520 nm, while Ag_3PO_4/CNFs-2 (Figure 7c) could show relatively weak absorption in the visible region. Thus, these results indicated that Ag_3PO_4/CNFs-1 sample could absorb more photon and might prove itself as a more favorable photocatalyst with enhanced activity.

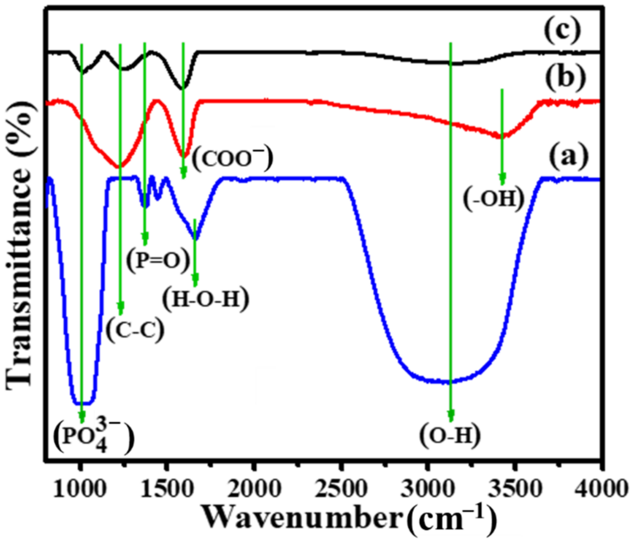

Figure 6. FTIR spectra; (**a**) Ag_3PO_4 powder, (**b**) acid-treated CNFs, and (**c**) Ag_3PO_4/CNFs-1 heterostructure.

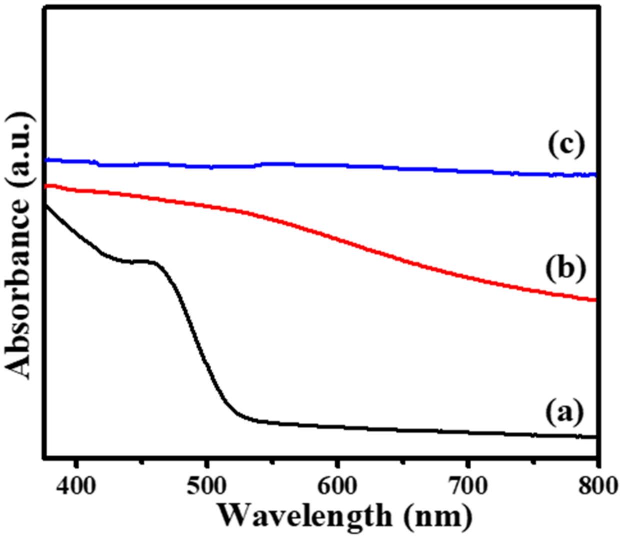

Figure 7. Uv-vis diffuse reflectance spectra; (**a**) Ag_3PO_4 powder, (**b**) Ag_3PO_4/CNFs-2 heterostructure, and (**c**) Ag_3PO_4/CNFs-1 heterostructure.

Results of photocatalytic performances exhibited by different photocatalysts towards the photodegradation of MB dye solution under simulated solar light irradiation are shown in Figure 8a. In order to evaluate the absorption property of electrospun CNFs, an experiment was carried out under similar conditions using bare CNFs, which showed negligible absorption of MB. The degradation is represented as the variation of (C/C_0) with irradiation time, where C_0 and C are the concentrations of dye solution at the initial time and at time t, respectively. When using P25 as the standard photocatalyst, only ~38% of MB dye solution was degraded in 50 min, indicating a low photocatalytic activity of P25. Similarly, the degradation results showed that less than 95% of MB dye solution was degraded within 50 min utilizing Ag_3PO_4 powder and Ag_3PO_4/CNFs-2 heterostructure. Contrastingly, more than 98% of dye solution was degraded within 40 min utilizing Ag_3PO_4/CNFs-1 heterostructure. Here, we believe that the higher photocatalytic efficiency of Ag_3PO_4/CNFs-1 heterostructure than that of Ag_3PO_4/CNFs-2 heterostructure is attributed to the strong uniformity and smaller Ag_3PO_4 particles dispersed on CNFs offering high level of exposure. Additionally, the lower photocatalytic activity of Ag_3PO_4 powder may refer to its low solubility and photocorrosion [48]. Furthermore, the enhanced photocatalytic activity of

Ag_3PO_4/CNFs heterostructures can be assigned to the synergistic effect between Ag_3PO_4 and CNFs due to their interfacial adhesion, which leads to the migration of excited electron from conduction band (CB) of Ag_3PO_4 to CNFs. As mentioned earlier [28,29], CNFs exhibit good conductivity and can act as an electron sink to prevent the recombination of photogenerated charge carriers [30]. Hence, this transfer phenomenon of electrons from CB of Ag_3PO_4 to CNFs could protect Ag_3PO_4 from photocorrosion, as shown in Formula (1) [25].

$$Ag^{+} + e^{-} \longrightarrow Ag \qquad (1)$$

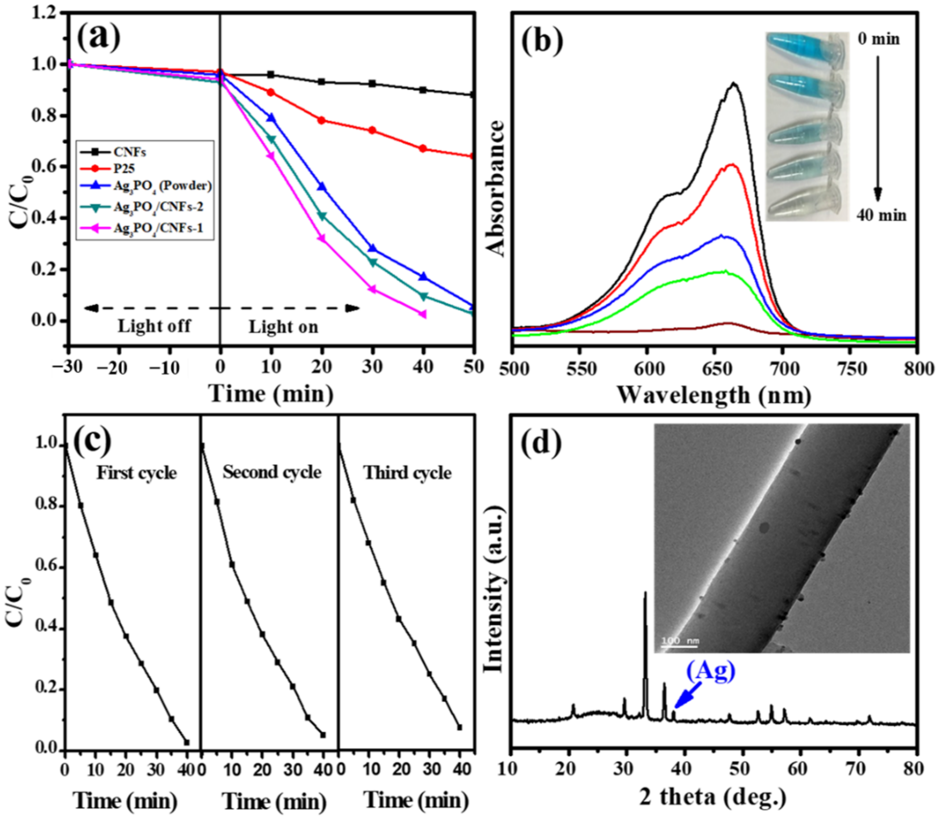

Figure 8. (**a**) Photocatalytic performances of CNFs, P25, Ag_3PO_4 powder, and Ag_3PO_4/CNFs heterostructures towards the photodegradation of MB solution; (**b**) absorbance variation of MB solution utilizing Ag_3PO_4/CNFs-1heterostructure; (**c**) cyclic photocatalytic performances of Ag_3PO_4/CNFs-1heterostructure, and (**d**) XRD pattern of used Ag_3PO_4/CNFs-1heterostructure. Insets; (**b**) digital photo of change in color of MB solution corresponding to degradation times and (**d**) TEM image of nanofiber of used Ag_3PO_4/CNFs-1 heterostructure.

The absorbance variations of MB solution utilizing Ag_3PO_4/CNFs-1 heterostructure under visible light irradiation at different times are shown in Figure 8b. The absorbance peak corresponding to MB at 665 nm is diminished gradually with the increase in irradiation time. At the same time, the color of MB dye solution also gradually diminished in presence of Ag_3PO_4/CNFs-1 heterostructure, as shown in inset, Figure 8b. Furthermore, the maximum absorption wave lengths of MB were not shifted, which indicated that the benzene/heterocyclic ring was decomposed rather than the simple decoloration process [49]. Moreover, the stability of the photocatalyst was evaluated by conducting a cycle test for the degradation of MB solution. For this purpose, used sample was separated by centrifugation and dried at room temperature then applied again for the degradation process under similar conditions. From the results (Figure 8c), it was found that the Ag_3PO_4/CNFs-1 heterostructure could work as a stable and efficient visible light photocatalyst up to the third cycle; however, there was a decrease in the activity during the recycling reaction, which might be attributed to the loss of photocatalyst during cycling experiments.

Moreover, to elucidate the structural integrity of photocatalyst, XRD analysis and TEM characterization of used Ag_3PO_4/CNFs-1 heterostructure were performed. Figure 8d depicts the XRD pattern of the Ag_3PO_4/CNFs-1 heterostructure after the third time cyclic test. As shown in the XRD pattern, an additional minor diffraction peak of metallic Ag appeared along with the corresponding diffraction peaks of Ag_3PO_4 and CNFs indicating the partial reduction of Ag_3PO_4 during the cyclic process. Additionally, the TEM image (inset, Figure 8d) of nanofiber of used Ag_3PO_4/CNFs-1 heterostructure showed its integrity even after three cycle tests without a significant loss of nanoparticles.

From the above discussions and results, it can be supposed that the CNFs play a key role in enhancing the photocatalytic activity and stability of Ag_3PO_4. However, the exact mechanism for the photocatalytic degradation of MB dye solution by Ag_3PO_4/CNFs heterostructures still needs further study; we have proposed a possible mechanism as shown in the schematic illustration (Figure 9) based on the above discussion and previous reports [13,50]. Under visible light irradiation, electrons (e^-) from the valance band (VB) of Ag_3PO_4 become excited due to the conduction band (CB) generating electron–hole (e^-–h^+) pairs (photogenerated charge carriers). During the photochemical reaction, the excited electrons in the CB of Ag_3PO_4 can ultimately migrate to the CNFs and react with adsorbed oxygen molecules to form $O_2^{\bullet-}$ radicals. At the same time, isolated h^+ can be utilized in the degradation of MB dye solution by direct oxidation, or it can react with water to produce $OH^\bullet$ radicals. Thus, the obtained reactive oxygen species (ROS) $O_2^{\bullet-}$ and $OH^\bullet$ radicals as well as holes (h^+) ultimately oxidize MB dye solution. The possible photochemical reactions taking place can be summarized by Formula (2)–(7) as follows:

$$Ag_3PO_4 \xrightarrow{h\upsilon} h^+(VB) + e^-(CB) \tag{2}$$

$$Ag_3PO_4(e^-_{CB}) + O_2 \longrightarrow Ag_3PO_4 + O_2^{\bullet\,-} \tag{3}$$

$$Ag_3PO_4(h^+_{VB}) + OH^- \longrightarrow Ag_3PO_4 + OH^\bullet \tag{4}$$

$$Ag_3PO_4(e^-_{CB}) + CNFs \longrightarrow Ag_3PO_4 + CNFs\ (e^-) \tag{5}$$

$$CNFs\ (e^-) + O_2 \longrightarrow CNFs + O_2^{\bullet\,-} \tag{6}$$

$$h^+/OH^\bullet/O_2^{\bullet\,-} + \text{dye solution} \longrightarrow \text{degradation} \tag{7}$$

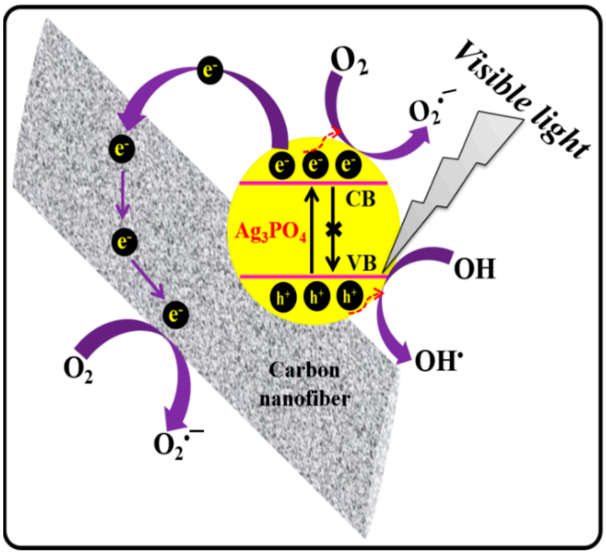

Figure 9. Schematic illustration for the photodegradation of MB solution using proposed Ag_3PO_4/CNFs heterostructure.

4. Conclusions

In summary, with the aid of electrospinning and the carbonization process, two types of Ag_3PO_4/CNFs heterostructures are fabricated. FESEM and TEM analyses revealed the uniform distribution of small crystalline Ag_3PO_4 nanoparticles on the surface of CNFs in the Ag_3PO_4/CNFs heterostructure obtained by the colloidal synthesis approach (Ag_3PO_4/CNFs-1). Contrastingly, bigger-sized Ag_3PO_4 nanoparticles were found to be distributed on the surface of CNFs with remarkable agglomeration in the Ag_3PO_4/CNFs heterostructure obtained by the precipitation synthesis approach (Ag_3PO_4/CNFs-2). Photocatalytic investigation of both the formulations towards the degradation of MB solution under visible light irradiation suggested that Ag_3PO_4/CNFs-1 is more advantageous over Ag_3PO_4/CNFs-2. Additionally, Ag_3PO_4/CNFs heterostructures could be easily separated from solution after use by sedimentation caused due to the high length-to-diameter ratio of CNFs. Finally, it is believed that the Ag_3PO_4/CNFs-1 heterostructure possessing enhanced photocatalytic performances will promote its practical application to remove organic pollutants from wastewater.

Author Contributions: For this research articles, the individual contribution of author was as follows: conceptualization and data analysis, G.P.; methodology, G.P.; writing—original draft preparation, G.P.; writing—reviewing and editing, G.P. and M.P.; resource and supervision, M.P.; funding acquisition, M.P. All authors have read and agreed to the published version of the manuscript.

Funding: This research was supported by the Traditional Culture Convergence Research Program through the National Research Foundation of Korea (NRF) funded by the Ministry of Science, ICT and Future Planning (2018M3C1B5052283). This work was also supported by the National Research Foundation of Korea (NRF) grant funded by the Korea government (MSIT) (No. NRF2019R1A2C1004467).

Institutional Review Board Statement: Not applicable.

Informed Consent Statement: Not applicable.

Conflicts of Interest: The authors declare no conflict of interest.

References

1. Hoffmann, M.R.; Martin, S.T.; Choi, W.; Bahnemannt, D.W. Environmental Applications of Semiconductor Photocatalysis. *Chem. Rev.* **1995**, *95*, 69–96. [CrossRef]
2. Fujishima, A.; Honda, K. Electrochemical photolysis of water at a semiconductor electrode. *Nature* **1972**, *238*, 37–38. [CrossRef]
3. Livraghi, S.; Paganini, M.C.; Giamello, E.; Selloni, A.; Valentin, C.D.; Pacchioni, G. Origin of photoactivity of nitrogen-doped titanium dioxide under visible light. *J. Am. Chem. Soc.* **2006**, *128*, 15666–15671. [CrossRef]
4. Yu, J.G.; Yu, X.X.; Huang, B.B.; Zhang, X.Y.; Dai, Y. Hydrothermal synthesis and visible-light photocatalytic activity of novel cage-like ferric oxide hollow spheres. *Cryst. Growth. Des.* **2009**, *9*, 1474–1480. [CrossRef]
5. Li, Q.; Guo, B.; Yu, J.; Ran, J.; Zhang, B.; Yan, H.; Gong, J.R. Highly efficient visible-light-driven photocatalytic hydrogen production of CdS-cluster-decorated graphene nanosheets. *J. A. Chem. Soc.* **2011**, *133*, 10878–10884. [CrossRef]
6. Panthi, G.; Yousef, A.; Barakat, N.A.M.; Khalil, K.A.; Akhter, S.; Choi, Y.; Kim, H.Y. Mn_2O_3/TiO_2 nanofibers with broad-spectrum antibiotics effect and photocatalytic activity for preliminary stage of water desalination. *Ceram. Int.* **2013**, *39*, 2239–2246. [CrossRef]
7. Zhao, D.; Chen, C.C.; Wang, Y.; Ma, W.H.; Zhao, J.C.; Rajh, T.; Zang, L. Enhanced photocatalytic degradation of dye pollutants under visible irradiation on Al (III)-modified TiO_2: Structure, interaction, and interfacial electron transfer. *Environ. Sci. Technol.* **2008**, *42*, 308–314. [CrossRef] [PubMed]
8. Panthi, G.; Kwon, O.H.; Kuk, Y.S.; Gyawali, K.R.; Park, Y.W.; Park, M. Ternary Composite of Co-Doped CdSe@electrospun Carbon Nanofibers: A Novel Reusable Visible LightDriven Photocatalyst with Enhanced Performance. *Catalysts* **2020**, *10*, 348. [CrossRef]
9. Wang, Z.; Ci, X.B.; Dai, H.J.; Yin, L.; Shi, H.X. One-step synthesis of highly active Ti-containing Cr-modified MCM-48 mesoporous material and the photocatalytic performance for decomposition of H_2S under visible light. *Appl. Surf. Sci.* **2012**, *258*, 8258–8263. [CrossRef]
10. Tang, J.T.; Gong, W.; Cai, T.J.; Xie, T.; Deng, C.; Peng, Z.H.; Deng, Q. Novel visible light responsive Ag@(Ag_2S/Ag_3PO_4) photocatalysts: Synergistic effect between Ag and Ag_2S for their enhanced photocatalytic activity. *RSC. Adv.* **2013**, *3*, 2543–2547. [CrossRef]
11. Yi, Z.; Ye, J.; Kikugawa, N.; Kako, T.; Ouyang, S.; Williams, H.S.; Yang, H.; Cao, J.; Luo, W.; Li, Z. An orthophosphate semiconductor with photooxidation properties under visible-light irradiation. *Nat. Mater.* **2010**, *9*, 559–564. [CrossRef]

12. Wan, J.; Liu, E.; Fan, J.; Hu, X.; Sun, L.; Tang, C.; Yin, Y.; Li, H.; Hu, Y. In-situ synthesis of plasmonic Ag/Ag_3PO_4 tetrahedron with exposed {111} facets for high visible-light photocatalytic activity and stability. *Ceram. Int.* **2015**, *41*, 6933–6940. [CrossRef]
13. Panthi, G.; Park, S.J.; Chae, S.H.; Kim, T.W.; Chung, H.J.; Hong, S.T.; Park, M.; Kim, H.Y. Immobilization of Ag3PO4 nanoparticles on electrospun PAN nanofibers via surface oximation: Bifunctional composite membrane with enhanced photocatalytic and antimicrobial activities. *J. Ind. Eng. Chem.* **2017**, *45*, 277–286. [CrossRef]
14. Panthi, G.; Barakat, N.A.M.; Park, M.; Kim, H.K.; Park, S.J. Fabrication of PdS/ZnS NPs doped PVAc hybrid electrospun nanofibers: Effective and reusable catalyst for dye photodegradation. *J. Ind. Eng. Chem.* **2015**, *21*, 298–302. [CrossRef]
15. Yang, X.F.; Cui, H.Y.; Li, Y.; Qin, J.L.; Zhang, R.X.; Tang, H. Fabrication of Ag_3PO_4-Graphene Composites with Highly Efficient and Stable Visible Light Photocatalytic Performance. *ACS Catal.* **2013**, *3*, 363–369. [CrossRef]
16. Tang, J.T.; Liu, Y.H.; Li, H.Z.; Tan, Z.; Li, D.T. A novel Ag_3AsO_4 visible-light-responsive photocatalyst: Facile synthesis and exceptional photocatalytic performance. *Chem. Commun.* **2013**, *49*, 5498–5500. [CrossRef] [PubMed]
17. Panthi, G.; Gyawali, K.R.; Park, M. Towards the Enhancement in Photocatalytic Performance of Ag3PO4 Nanoparticles through Sulfate Doping and Anchoring on Electrospun Nanofibers. *Nanomaterials* **2020**, *10*, 929. [CrossRef] [PubMed]
18. Xu, J.W.; Gao, Z.D.; Han, K.; Liu, Y.; Song, Y.Y. Synthesis of Magnetically Separable $Ag_3PO_4/TiO_2/Fe_3O_4$ Heterostructure with Enhanced Photocatalytic Performance under Visible Light for Photoinactivation of Bacteria. *ACS Appl. Mater. Interfaces* **2014**, *6*, 15122–15131. [CrossRef]
19. Yao, W.; Zhang, B.; Huang, C.; Ma, C.; Song, X.; Xu, Q. Synthesis and characterization of high efficiency and stable Ag_3PO_4/TiO_2 visible light photocatalyst for the degradation of methylene blue and rhodamine B solutions. *J. Mater. Chem.* **2012**, *22*, 4050–4055. [CrossRef]
20. Dong, C.; Wu, K.L.; Li, M.R.; Liu, L.; Wei, X.W. Synthesis of Ag_3PO_4-ZnO nanorod composites with high visible-light photocatalytic activity. *Catal. Commun.* **2014**, *46*, 32–35. [CrossRef]
21. Yang, X.; Qin, J.; Jiang, Y.; Li, R.; Li, Y.; Tang, H. Bifunctional TiO_2/Ag_3PO_4/graphene composites with superior visible light photocatalytic performance and synergistic inactivation of bacteria. *RSC Adv.* **2014**, *4*, 18627–18636. [CrossRef]
22. Liu, L.; Liu, J.; Sun, D.D. Graphene oxide enwrapped Ag_3PO_4 composite: Towards a highly efficient and stable visible-light-induced photocatalyst for water purification. *Catal. Sci. Technol.* **2012**, *2*, 2525–2532. [CrossRef]
23. Liang, Q.; Shi, Y.; Ma, W.; Li, Z.; Yang, X. Enhanced photocatalytic activity and structural stability by hybridizing Ag_3PO_4 nanospheres with graphene oxide sheets. *Phys. Chem. Chem. Phys.* **2012**, *14*, 15657–15665. [CrossRef]
24. Wang, Z.; Yin, L.; Zhang, M.; Zhou, G.; Fei, H.; Shi, H.; Dai, H. Synthesis and characterization of Ag_3PO_4/multiwalled carbon nanotube composite photocatalyst with enhanced photocatalytic activity and stability under visible light. *J Mater. Sci.* **2014**, *49*, 1585–1593. [CrossRef]
25. Xu, H.; Wang, C.; Song, Y.; Zhu, J.; Xu, Y.; Yan, J.; Song, Y.X.; Li, H. CNT/Ag_3PO_4 composites with highly enhanced visible light photocatalytic activity and stability. *Chem. Eng. J.* **2014**, *241*, 35–42. [CrossRef]
26. Ma, J.; Zou, J.; Li, L.; Yao, C.; Kong, Y.; Cui, B.; Zhu, R.; Li, D. Nanocomposite of attapulgite-Ag_3PO_4 for Orange II photodegradation. *Appl. Catal. B Environ.* **2014**, *144*, 36–40. [CrossRef]
27. Chen, P.; Zhang, L.; Wu, Q.; Yao, W. Novel Synthesis of Ag3PO4/CNFs/Silica-fiber hybrid composite as an efficient photocatalyst. *J. Taiwan Inst. Chem. Eng.* **2016**, *63*, 506–511. [CrossRef]
28. Unalan, H.; Wei, D.; Suzuki, K.; Dalal, S.; Hiralal, P.; Matsumoto, H.; Imaizumi, S.; Minagawa, M.; Tanioka, A.; Flewitt, A.; et al. Photoelectrochemical cell using dye sensitized zinc oxide nanowires grown on carbon fibers. *Appl. Phys. Lett.* **2008**, *93*, 133116–133118. [CrossRef]
29. Mu, J.; Shao, C.; Guo, Z.; Zhang, Z.; Zhang, M.; Zhang, P.; Chen, B.; Liu, Y. High Photocatalytic Activity of ZnO-Carbon Nanofiber Heteroarchitectures. *ACS Appl. Mater Interfaces* **2011**, *3*, 590–596. [CrossRef]
30. Mu, J.; Shao, C.; Guo, Z.; Zhang, M.; Zhang, Z.; Zhang, P.; Chen, B.; Liu, Y.N. In_2O_3 nanocubes/carbon nanofibers heterostructures with high visible light photocatalytic activity. *J. Mater. Chem.* **2012**, *22*, 1786–1793. [CrossRef]
31. Lee, J.S.; Kwon, O.S.; Park, S.J.; Park, E.Y.; You, S.A.; Yoon, H.; Jang, J. Fabrication of Ultrafine Metal-Oxide-Decorated Carbon Nanofibers for DMMP Sensor Application. *ACS Nano* **2011**, *5*, 7992–8001. [CrossRef]
32. Lakshminarayanan, P.V.; Toghiani, H.; Pittman, C.U., Jr. Nitric acid oxidation of vapor grown carbon nanofibers. *Carbon* **2004**, *42*, 2433–2442. [CrossRef]
33. Seo, M.K.; Park, S.J. Influence of air-oxidation on electric double layer capacitances of multi-walled carbon nanotube electrodes. *Curr. Appl. Phys.* **2010**, *10*, 241–244. [CrossRef]
34. Okajima, K.; Ohta, K.; Sudoh, M. Capacitance behavior of activated carbon fibers with oxygen-plasma treatment. *Electrochim. Acta* **2005**, *50*, 2227–2231. [CrossRef]
35. Oh, H.S.; Kim, K.; Ko, Y.J.; Kim, H. Effect of chemical oxidation of CNFs on the electrochemical carbon corrosion in polymer electrolyte membrane fuel cells. *Int. J. Hydrog. Energy* **2010**, *35*, 701–708. [CrossRef]
36. Yu, H.; Jin, Y.; Peng, F. Kinetically Controlled Side-Wall Functionalization of Carbon Nanotubes by Nitric Acid Oxidation. *J. Phys. Chem. C* **2008**, *112*, 6758–6763. [CrossRef]
37. Khan, A.; Qamar, M.; Muneer, M. Synthesis of highly active visible-light-driven colloidal silver orthophosphate. *Chem. Phys. Lett.* **2012**, *519–520*, 54–58. [CrossRef]
38. Lafdi, K.; Wright, M.A. Carbon Fibers. In *Handbook of Composites*; Peters, S.T., Ed.; Chapman & Hall: London, UK, 1998.

39. Zhou, Z.; Lai, C.; Zhang, L.; Qian, Y.; Hou, H.; Reneker, D.H. Development of carbon nanofibers from aligned electrospun polyacrylonitrile nanofiber bundles and characterization of their microstructural, electrical, and mechanical properties. *Polymer* **2009**, *50*, 2999–3006. [CrossRef]
40. Liu, B.; Li, Z.; Xu, S.; Han, D.; Lu, D. Enhanced visible-light photocatalytic activities of Ag_3PO_4/MWCNT nanocomposites fabricated by facile in situ precipitation method. *J. Alloys Compd.* **2014**, *596*, 19–24. [CrossRef]
41. Miller, L.M.; Vairavamurthy, V.; Chance, M.R.; Mendelsohn, R.; Paschalis, E.P.; Betts, F.; Boskey, A.L. In situ analysis of mineral content and crystallinity in bone using infrared micro spectroscopy of the v4 $PO_4{}^{3-}$ vibration. *Biochim. Biophys. Acta Gen. Subj.* **2001**, *1527*, 11–19. [CrossRef]
42. Moustafa, Y.M.; El-Egili, K. Infrared studies on the structure of sodium phosphate glasses. *J. Non-Cryst. Solids* **1998**, *240*, 144–153. [CrossRef]
43. Tang, T.; Shi, Z.; Yin, J. Poly(benzimidazole) functionalized multi-walled carbon nanotubes/100% acidified poly(hydroxyaminoether) composites: Synthesis, characterization and properties. *Mater. Chem. Phys.* **2011**, *129*, 356–364. [CrossRef]
44. Qin, Y.H.; Yang, H.H.; Zhang, X.S.; Li, P.; Zhou, X.G.; Niu, L.; Yuan, W.K. Electrophoretic deposition of network like carbon nanofibers as a palladium catalyst support for ethanol ixidation in alkaline media. *Carbon* **2010**, *48*, 48–3323. [CrossRef]
45. Mawhinney, D.; Naumenko, V.; Kuznetsova, A.; Yates, J.; Liu, J.R. Smalley, Infrared Spectral Evidence for the Etching of Carbon Nanotubes: Ozone Oxidation at 298 K. *J. Am. Chem. Soc.* **2000**, *122*, 2383–2384. [CrossRef]
46. Zhu, C.; Guo, S.; Wang, P.; Xing, L.; Fang, Y.; Zhai, Y.; Dong, S. One-pot, water-phase approach to high-quality graphene/TiO_2 composite nanosheets. *Chem. Commun.* **2010**, *46*, 7148–7150. [CrossRef] [PubMed]
47. Panthi, G.; Ranjit, R.; Kim, H.Y.; Mulmi, D.D. Size dependent optical and antibacterial properties of Ag_3PO_4 synthesized by facile precipitation and colloidal approach in aqueous solution. *Optik* **2018**, *156*, 60–68. [CrossRef]
48. Lv, Y.; Huang, K.; Zhang, W.; Yang, B.; Chi, F.; Ran, S.; Liu, X. One step synthesis of Ag/Ag_3PO_4/$BiPO_4$ double-heterostructured nanocomposites with enhanced visible-light photocatalytic activity and stability. *Ceram. Int.* **2015**, *40*, 8087–8092. [CrossRef]
49. Panthi, G.; Park, M.; Park, S.J.; Kim, H.K. PAN electrospun nanofibers reinforced with Ag_2CO_3 nanoparticles: Highly efficient visible light photocatalyst for photodegradation of Organic Contaminants in waste water. *Macromol. Res.* **2015**, *23*, 149–155. [CrossRef]
50. Dong, P.Y.; Wang, Y.H.; Cao, B.C.; Xin, S.Y.; Guo, L.N.; Zhang, J.; Li, F.H. Ag_3PO_4/reduced graphite oxide sheets nanocomposites with highly enhanced visible light photocatalytic activity and stability. *Appl. Catal. B Environ.* **2013**, *132–133*, 45–53. [CrossRef]